

Accepted Manuscript

Identification and Structure Activity Relationships of Quinoline Tertiary Alcohol Modulators of ROR γ t

David A. Kummer, Maxwell D. Cummings, Marta Abad, Joseph Barbay, Glenda Castro, Ronald Wolin, Kevin D. Kreutter, Umar Maharroof, Cynthia Milligan, Rachel Nishimura, Joan Pierce, Celine Schalk-Hihi, John Spurlino, Maud Urbanski, Hariharan Venkatesan, Aihua Wang, Craig Woods, Xiaohua Xue, James P. Edwards, Anne M. Fourie, Kristi Leonard

PII: S0960-894X(17)30163-4
DOI: <http://dx.doi.org/10.1016/j.bmcl.2017.02.044>
Reference: BMCL 24716

To appear in: *Bioorganic & Medicinal Chemistry Letters*

Received Date: 17 January 2017
Revised Date: 10 February 2017
Accepted Date: 14 February 2017

Please cite this article as: Kummer, D.A., Cummings, M.D., Abad, M., Barbay, J., Castro, G., Wolin, R., Kreutter, K.D., Maharroof, U., Milligan, C., Nishimura, R., Pierce, J., Schalk-Hihi, C., Spurlino, J., Urbanski, M., Venkatesan, H., Wang, A., Woods, C., Xue, X., Edwards, J.P., Fourie, A.M., Leonard, K., Identification and Structure Activity Relationships of Quinoline Tertiary Alcohol Modulators of ROR γ t, *Bioorganic & Medicinal Chemistry Letters* (2017), doi: <http://dx.doi.org/10.1016/j.bmcl.2017.02.044>

This is a PDF file of an unedited manuscript that has been accepted for publication. As a service to our customers we are providing this early version of the manuscript. The manuscript will undergo copyediting, typesetting, and review of the resulting proof before it is published in its final form. Please note that during the production process errors may be discovered which could affect the content, and all legal disclaimers that apply to the journal pertain.



Identification and Structure Activity Relationships of Quinoline Tertiary Alcohol Modulators of ROR γ t

Authors: David A. Kummer^{*,a}, Maxwell D. Cummings^{*,b}, Marta Abad^b, Joseph Barbay^c, Glenda Castro^a, Ronald Wolin^a, Kevin D. Kreutter^c, Umar Maharroof^c, Cynthia Milligan^b, Rachel Nishimura^a, Joan Pierce^c, Celine Schalk-Hihi^b, John Spurlino^b, Maud Urbanski^c, Hariharan Venkatesan^a, Aihua Wang^c, Craig Woods^a, Xiaohua Xue^a, James P. Edwards^a, Anne M. Fourie^a, Kristi Leonard^{*,c}

Corresponding authors: mcummin1@its.jnj.com (M. Cummings), dkummer1@its.jnj.com (D. Kummer), kleonar1@its.jnj.com (K. Leonard).

Addresses:

^aDiscovery Immunology, Janssen Research and Development, 3210 Merryfield Row, San Diego, CA 92121

^bDiscovery Sciences, Janssen Research and Development, Welsh and McKean Roads, Spring House, PA 19477

^cDiscovery Immunology, Janssen Research and Development, Welsh and McKean Roads, Spring House, PA 19477

Keywords. ROR γ t, retinoic acid-related orphan nuclear receptor gamma t, agonist, neutral antagonist, inverse agonist, Th17, IL-17

Abstract. A high-throughput screen of the ligand binding domain of the nuclear receptor retinoic acid-related orphan receptor gamma t (ROR γ t) employing a thermal shift assay yielded a quinoline tertiary alcohol hit. Optimization of the 2-, 3- and 4-positions of the quinoline core using structure-activity relationships and structure-based drug design methods led to the

discovery of a series of modulators with improved ROR γ t inhibitory potency and inverse agonism properties.

The retinoic acid-related orphan receptor (ROR) family of nuclear receptors comprises three members: ROR α , ROR β and ROR γ , with each member generating multiple isoforms. The ROR γ isoform is widely expressed in many tissues including kidney, adipose, liver and skeletal muscle, whereas the ROR γ t isoform is only expressed in a few distinct cell types of the immune system.¹ ROR γ t is the key transcription factor that drives the differentiation of naïve CD4⁺ T helper cells to Th17 cells, and induces the transcription of IL-17A and IL-17F.² There is abundant evidence that IL-17A and the Th17 pathway play an important role in the pathogenesis of psoriasis³ and biologics known to inhibit the Th17/IL-17 pathway are clinically validated for the treatment of psoriasis.⁴ Due to its effect on Th17 cells, ROR γ t may also play a role in the development of diseases such as rheumatoid arthritis,^{5,6} inflammatory bowel disease,⁷ and multiple sclerosis.⁸ Therefore, targeting the inhibition of Th17 differentiation and IL-17 production through modulation of ROR γ t with small molecules has generated much interest in drug discovery research.⁹⁻¹²

For nuclear receptors such as ROR γ t, transcriptional activity can be modulated by the binding of small molecule effectors to the ligand binding domain, and several mechanisms could affect this activity.¹³ In the first scenario, small molecule effectors can bind to the nuclear receptor and induce a conformational change that enhances binding of a co-activator peptide to the nuclear receptor. These ligands would be considered agonists and binding should result in an increase in

ROR γ t-driven gene transcription.¹⁴ Secondly, small molecule effectors can also bind to the nuclear receptor and induce a conformation that yields enhanced binding of a co-repressor peptide to the nuclear receptor. These ligands would be considered inverse agonists and binding should lead to decreased gene transcription.¹⁵ Finally, ligands may also bind to the nuclear receptor and induce a conformational change that precludes co-activator or co-repressor peptide binding. These ligands could have various functional activities including inverse agonism or neutral antagonism, the latter term referring to compounds that bind to the nuclear receptor with no functional response.^{10,13}

Early crystal structures of the ROR γ t ligand binding domain (LBD¹⁶) complexed with the agonist 25-hydroxycholesterol¹⁷ and with the inverse agonist digoxin^{17,18} revealed structural details of the binding interactions for these effector molecules. When bound, the agonist 25-hydroxycholesterol is completely buried in the center of the LBD. Interestingly, the bound sterol makes no direct contact with the bound co-activator peptide¹⁷ (Figure 1a). Helix 12 of the LBD is a key structural element of the co-activator peptide binding site, and the bound sterol makes indirect contact with Tyr502 of helix 12 via a water-bridged hydrogen bond. The bound sterol also approaches the imidazole of His479 in helix 11, and His479 in turn is involved in close contacts with the sidechains of both Tyr502 and Phe506 of helix 12¹⁷ (see also Figure 1a). Additionally, and of particular relevance to the present work, a previous small-molecule study suggested a key mechanistic role for His479 in synthetic effector function.¹⁹ Bound digoxin also occupies the sterol binding site of the LBD, with the trisaccharide moiety extending well beyond the region occupied by the alcohol-bearing side chain of the bound sterol.²⁰ This binding mode forces helix 10/11 out of the agonist conformation observed in the sterol complex structure, and

this adjustment in turn likely precludes helix 12 from adopting the observed agonist conformation. Thus, binding of digoxin causes conformational adjustments that inhibit co-activator binding (Figure 1b).

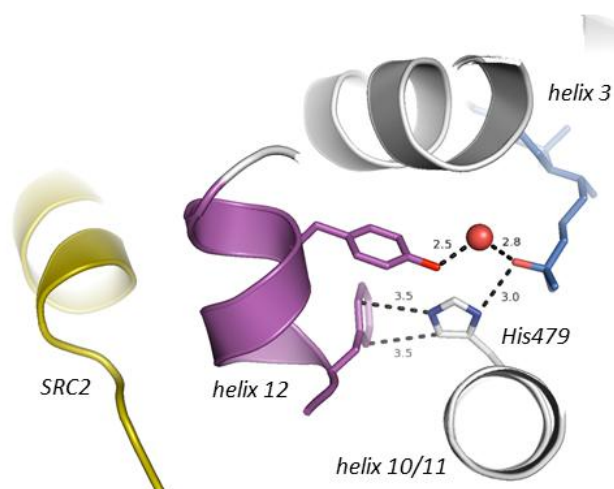


Figure 1a. Interactions of His479 in the sterol agonist complex structure.¹⁷ A view down the axis of helix 10/11 of the LBD with the imidazole of His479 projecting toward both the bound sterol (blue color-by-atom) and helix 12 of the LBD (PDB ID 3L0L). His479 of helix 10/11 and Tyr502 and Phe506 of helix 12 participate in specific binding contacts related to the positioning of helix 12 in the co-activator peptide (SRC2) binding site. The oxygen of a bound water molecule is shown as a red sphere, and several intermolecular contacts are highlighted with dashed lines and with the intermolecular atom-atom distances shown.

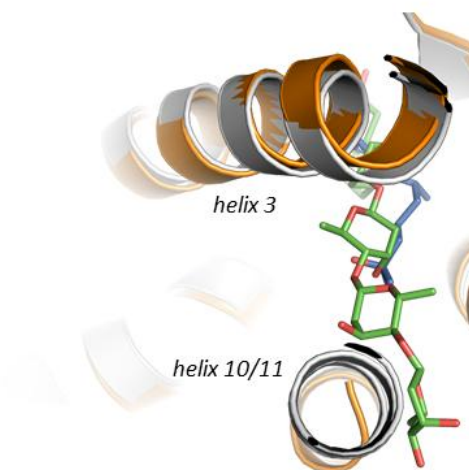


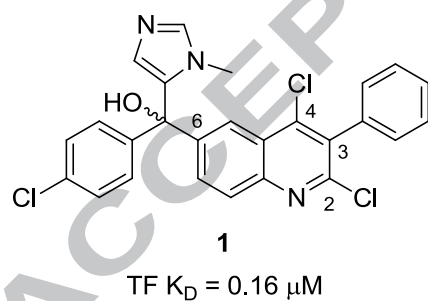
Figure 1b. Bound digoxin clashes with the agonist conformation of helix 10/11. A view of superimposed digoxin²⁰ (PDB ID 3B0W) and sterol¹⁷ (PDB ID 3L0L) LBD complexes. Helix 11 of the LBD (projecting toward the viewer) is disordered in the digoxin complex (LBD: orange; digoxin: green color-by-atom), in contrast to what is observed in the sterol complex (LBD: white; sterol: blue color-by-atom).

In this report we describe the structure-activity relationships (SAR) and structure-based optimization of the 2-, 3- and 4-positions of a series of quinoline tertiary alcohol ROR γ t modulators that act through binding at the sterol binding site of the LBD. Modification of these molecules leads to changes in potency and functional activity, with compounds showing agonism, inverse agonism, and neutral antagonism. The goal of our program was to identify

potent modulators of ROR γ t that would maintain a full inverse agonism profile in our functional assays.

Quinoline **1** (Figure 2) was identified from a high-throughput, thermal-shift-based assay using ThermoFluor[®] (TF) technology.^{21,22} In order to establish the SAR around this hit, we employed a TF binding assay using the ROR γ t LBD²² and a 1-hybrid cell-based functional reporter assay.²² Compounds of interest were then tested in a Th17 cell-based assay measuring IL-17A production to confirm activity in primary cells. Our optimization effort ultimately led to the discovery of high affinity ROR γ t modulators encompassing a range of functional activities. Herein we describe SAR data for substitution on the 2-, 3- and 4-positions of the quinoline core; future reports will disclose our efforts around other positions of this chemotype.

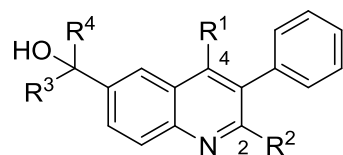
Figure 2. Racemic quinoline tertiary alcohol **1** was identified using a TF binding assay.

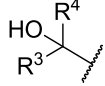
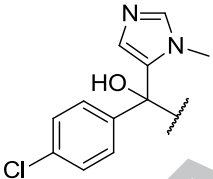
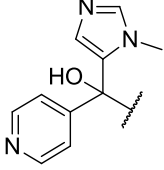
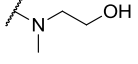


Our initial work on the hit **1** focused on exploring the SAR of the C2- and C4-positions of the quinoline core. Compound **1** contains a stereocenter at the carbon bearing the tertiary alcohol

group and was initially characterized as a mixture of stereoisomers. In Table 1, we depict two sets of racemic quinoline compounds that contain distinct substituents on the C6-position of the quinoline; the first contains a 4-chlorophenyl/1-methyl-1*H*-imidazol-5-yl substituted alcohol (compounds **1-9**) and the second contains a 1-methyl-1*H*-imidazol-5-yl/pyridin-4-yl substituted alcohol (compounds **10-16**). Compounds **1** and **10** behaved as inverse agonists and exhibited full suppression of ROR γ t-driven transcriptional activity in the cell-based reporter assay. Similar results were observed when comparing compounds **4** and **11**, both of which contain a 2-methoxy group in place of the 2-chloro atom on the quinoline core; the compounds maintained full inverse agonism activity with >90% efficacy. Replacement of the chlorine atom with a hydrogen atom at either the 2-position (compound **3**) or the 4-position (compound **2**) reduced both binding affinity ($K_D > 4 \mu\text{M}$) and cell potency ($\text{IC}_{50} > 2 \mu\text{M}$). However, in several cases we were able to maintain or slightly improve potency while maintaining full inverse agonism activity by retaining the 4-chlorine atom and replacing the 2-chlorine atom with electron-withdrawing or electron-donating groups such as methoxy, cyano, trifluoromethyl, dimethyl- and diethyl amino groups (compounds **4, 6, 8, 12, 13**). Replacement of both the 2- and 4-chlorine atoms with trifluoromethyl (compound **9**) showed a 16-fold increase in TF binding but only a 2-fold increase in cellular potency in the reporter assay, whereas 2,4-dicyanoquinoline **7** had a slight increase in TF binding with no effect on cell potency or efficacy. Also, modifications to the 4-position of compound **10** with dimethylamine (compound **15**) did not impact TF binding or cell potency, whereas methylamine (compound **16**) lost significant binding and cell potency.

Table 1. C2- and C4-quinoline SAR.^a

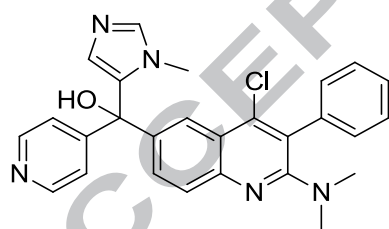


Cmpd ^b	C4-substituent (R ¹)	C2-substituent (R ²)		TF binding to RORγt LBD K _D (μM)	RORγt cell-based reporter assay IC ₅₀ (μM) (% inh ^c @ 6 μM)
1	Cl	Cl		0.16	0.26 (101)
2	H	Cl		>4 (57)	
3	Cl	H		4.3	2.7 (78)
4	Cl	OMe		0.1	0.22 (104)
5	OMe	OMe		0.57	~2 (97)
6	Cl	CN		0.051	0.11 (101)
7	CN	CN		0.055	0.24 (105)
8	Cl	CF ₃		0.057	0.12 (110)
9	CF ₃	CF ₃		0.0095	0.11 (97)
10	Cl	Cl			0.014
11	Cl	OMe	0.005		0.025 (92)
12	Cl	NMe ₂	0.002		0.0075 (105)
13	Cl	NEt ₂	0.002		0.011 (100)
14	Cl		15		1.9 (73)
15	NMe ₂	Cl	0.023		0.11 (101)
16	NHMe	Cl	9.5		>6 (17)

^aAll compounds are racemic mixtures. ^bCmpd = compound. ^cinh = inhibition.

After our initial efforts to probe the SAR with racemic material showed promise, methods were investigated to characterize the TF binding and modulation of ROR γ t-driven transcription in our cell-based reporter assay with individual enantiomers. This chemical series proved consistently amenable to isomer separation by supercritical fluid chromatography (SFC), and all isomeric mixtures were subsequently separated this way. The data in Table 2 shows that one enantiomer (**12a**) of compound **12** had significantly greater binding affinity in TF (145-fold) and greater potency in the cell-based reporter assay (56-fold) than the opposite enantiomer (**12b**). Interestingly, both enantiomers maintained full inverse agonism in the reporter assay. From this point forward, all compounds described in this manuscript are single enantiomers (absolute stereochemistry not determined) unless specifically indicated otherwise. The data described is for the more potent isomer with regard to binding to the LBD of ROR γ t as measured by the TF assay.

Table 2. Binding and cell-based activity of enantiomers of compound **12**.



Cmpd ^a	TF binding to ROR γ t LBD K _D (μ M)	ROR γ t reporter cell assay IC ₅₀ (μ M) (% inh ^d @ 6 μ M)
12^b	0.002	0.0075 (105)
12a^c	0.002	0.011 (105)
12b^c	0.29	0.62 (101)

^aCmpd = compound; ^bracemate; ^csingle enantiomer, absolute stereochemistry not determined; ^dinh = inhibition.

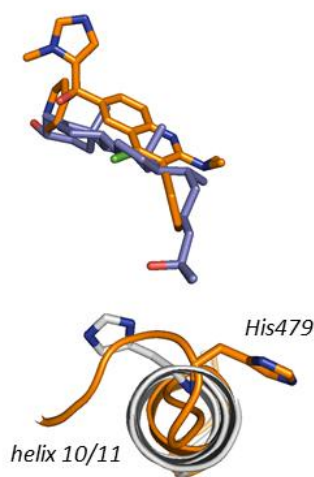
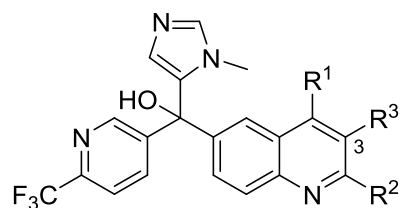


Figure 3. The (S) enantiomer of **12 binds in the sterol binding pocket.** The structure of the (S) enantiomer of **12** as positioned in the LBD complex (LBD: orange ribbon, orange color-by-atom; **12**(S): orange color-by-atom; deposited as PDB ID 5UFR) superimposed with the sterol agonist complex structure (LBD: white, white color-by-atom; sterol: purple color-by-atom; PDB ID 3L0L),¹⁷ viewed down the axis of helix 10/11. While the bound (S) enantiomer of **12** does not clash with the (superimposed) agonist conformation of the LBD, His479 is shifted from the conformation observed in the agonist complex.

Co-crystallization of ROR γ t LBD with racemate **12** yielded a 2.07Å resolution crystal structure of the S-enantiomer bound at the previously elucidated sterol binding site of the LBD (Figure

3).¹⁷ Interestingly, the overlay with the sterol agonist structure indicates that while the 3-phenyl group of the bound ligand does not cause an obvious steric clash with the agonist conformation of the LBD, the residues comprising helix 10/11 in the agonist structure are largely non-helical and His479 is shifted from the orientation observed in the agonist complex. The specific structural features of the small-molecule and binding interactions that drive this conformational change, and, in turn, presumably contribute to this compound behaving as a full inverse agonist in the reporter assay, remain unclear.

We next focused our chemistry effort on substitution at the C3-position of the quinoline core, in an effort to maximize chemical diversity while seeking to maintain full inverse agonism in our functional assay. Table 3 shows compounds that contain a 3-pyridyl-4-CF₃/1-methyl-1*H*-methylimidazol-5-yl tertiary alcohol at the C6-position of the quinoline, with varying substituents at the C3-position. Two examples containing a C3-phenyl group with potent TF binding affinity and full inverse agonism in the cell-based reporter assay are shown in compounds **17** and **18**. The cyanopyrimidine **19** demonstrates an example of a heterocyclic phenyl replacement that maintains full inverse agonism in the cell-based assay. Interestingly, the 4-(methylsulfonyl)phenyl substituted quinoline **20** maintained similar binding affinity ($K_D = 0.037 \mu\text{M}$) to that of compound **19**, but demonstrated functional agonism in the reporter assay, with an EC_{50} of $0.049 \mu\text{M}$ and stimulation of transcriptional activity of 78% at $6 \mu\text{M}$.

Table 3. Tertiary alcohol quinolines with varying substituents at the C3-position.^a

Cmpd ^b	R ¹	R ²	R ³	TF binding to ROR γ t LBD K _D (μ M)	ROR γ t cell-based reporter assay IC ₅₀ (μ M) (% inh. ^c @ 6 μ M)
17	OMe	CF ₃		0.015	0.19 (93)
18	Cl	azetidine		0.006	~0.05 (103)
19	Cl	OMe		0.032	0.31 (96)
20	Cl	OMe		0.037	0.049 (78%) ^d

^aAll compounds are single enantiomers, absolute stereochemistry not determined; ^bCmpd = compound; ^cinh = inhibition; ^ddenotes EC₅₀ (% increase in transcription activity).

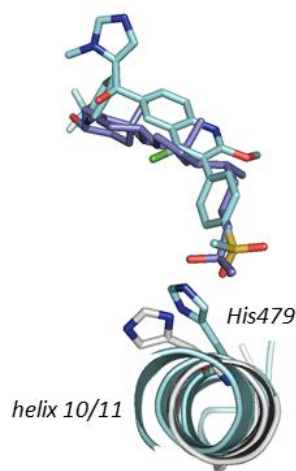


Figure 4. The quinoline tertiary alcohol **20 maintains a close-to-agonist conformation for His479.** The structure of the LBD-**20** complex (LBD: cyan, cyan color-by-atom; **20**: cyan color-by-atom; deposited as PDB ID 5UFO) superimposed with the sterol agonist complex structure (LBD: white, white color-by-atom; sterol: purple color-by-atom; PDB ID 3L0L),¹⁷ viewed along the helix 10/11 axis. In contrast to the LBD-**12** complex (Figure 3), bound **20** stabilizes His479 in a conformation very close to that seen in the sterol agonist complex.

Using x-ray crystallography conditions similar to those that yielded the initial complex structure with the (S)-enantiomer of **12**, we also succeeded in determining the 2.80Å resolution crystal structure of the functional agonist **20** bound to the LBD, which shows the (S)-enantiomer is bound in the complex. Relative to the sterol agonist structure, the LBD-**20** complex structure shows His479 shifted slightly toward the bound ligand, with the ligand sulfone oxygen in close

contact with the His479 sidechain (Figure 4). Helix 10/11 is fully resolved and completely helical, and overall is shifted slightly from its position in the sterol agonist complex. This contrasts with the inverse agonist complexes disclosed in this report (Figures 3 and 5), in which the residues comprising helix 10/11 in the agonist structure are resolved but largely or completely non-helical (see also eg. Ref. 19). The water-bridged hydrogen bond and ring-ring contacts with helix 12 observed in the sterol agonist complex are not observed in the LBD-20 complex structure (c.f. Figures 1a and 3). We hypothesize that the observed sulfone-imidazole contact serves to partially stabilize helix 10/11 in a “close to agonistic” conformation that allows or facilitates co-activator binding, thus contributing to agonistic function. These speculations are consistent with the observed complex structures and functional activities of these compounds.

While complicating the understanding of emerging SAR for a chemical series, overall it seems an attractive feature of a chemotype when a range of biological function can be achieved through relatively minor modifications of the parent structure, as noted here for these quinoline tertiary alcohols. Interestingly, similar behavior has been reported by other research groups working in the ROR γ t field.^{19,23}

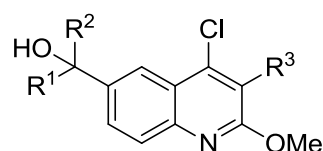
Medicinal chemistry efforts led us to exchange the 3-aryl group with 3-substituted benzylic groups. Structural and modeling studies later established that this targeted a slightly different region of the binding pocket, potentially allowing diverse substituents in close proximity to helix 10/11. Given the established importance of helices 10-12 for nuclear receptor function,²⁴ we were keenly interested in targeting interactions with this region of the LBD. Additionally,

modeling indicated that sufficient extension of a benzylic substituent could project out of the buried pocket and into a solvent-exposed region (c.f. digoxin, as in Figure 1b), thus providing an opportunity to incorporate more general chemical modifications aimed at modulating the physicochemical properties of these ligands. This design hypothesis was productive, with biaryl substituents proving particularly effective.

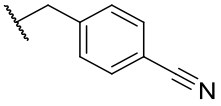
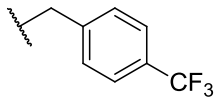
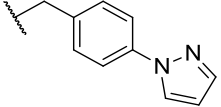
As shown in Table 4, data for compounds **21** and **22** indicates that unsubstituted or 4-fluorobenzyl groups are tolerated at the C3-position. Racemic mixture **21** and single enantiomer **22** were found to have binding affinities of 20 nM and 6.6 nM for ROR γ t, respectively. Although the C3-benzyl compounds **21** and **22** were potent binders in TF, they both showed only slight functional activity up to 6 μ M in the cellular reporter assay with partial impact on transcription, behaving as neutral antagonists at lower concentrations and partial inverse agonists at higher concentrations. Interestingly, the addition of larger substituents at the 4-benzyl position, such as trifluoromethyl and pyrazole (compounds **23** and **24**) resulted in single digit nanomolar binding affinities in TF and potency of 0.12 μ M and 0.089 μ M in the cellular reporter assay, respectively, while demonstrating a full inverse agonism profile. We also explored the C3-benzyl SAR with the 4-chlorophenyl/1-methyl-1*H*-imidazol-5-yl tertiary alcohol at the C6-position of the quinoline (Table 4). Similar to compounds **21** and **22**, 4-fluorobenzyl compound **25** was a neutral antagonist at lower concentrations with partial inverse agonism observed at high concentrations, whereas compounds **26-28**, containing a 4-cyano, -trifluoromethyl or -pyrazolyl group were all potent molecules displaying full inverse agonism.

The data clearly indicates that structural changes at the C3-position of the quinoline can have a dramatic effect on the transcriptional activity in the 1-hybrid cell-based reporter assay. It is interesting to observe the full spectrum of functional activities - agonism, neutral antagonism and inverse agonism, within this one chemical series. These results are consistent with the proximity of the C3 substituent of our ligands to helix 10/11, a structural element critical to the functional activity of the LBD.

Table 4. C3-benzyl SAR. All are single enantiomers except compound **21**.^a



Cmpd ^b			TF binding to ROR γ t LBD K _D (μ M)	ROR γ t cell-based reporter assay IC ₅₀ (μ M) (% inh. ^d @ 6 μ M)
21 ^c			0.020	>6 (20)
22			0.0066	~6 (42)
23			0.0015	0.12 (102)
24			0.005	0.089 (97)
25			0.012	~6 (62)

26		0.0062	0.14 (94)
27		0.0077	0.041 (103)
28		0.0092	0.073 (99)

^aAll compounds are single enantiomers unless otherwise denoted, absolute stereochemistry not determined; ^bCmpd = compound; ^cracemate; ^dinh = inhibition.

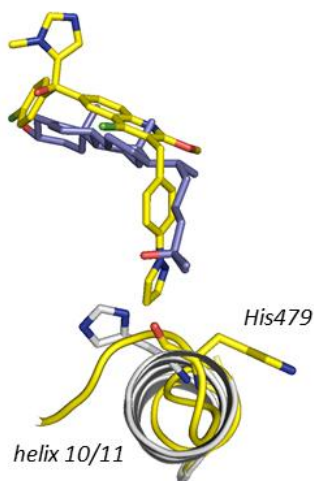


Figure 5. The 4-pyrazolylbenzyl quinoline **28** sterically clashes with helix 10/11. The structure of the LBD-**28** complex (LBD: yellow, yellow color-by-atom; **28**: yellow color-by-atom; deposited as PDB ID 5UHI) superimposed with the sterol agonist complex structure (LBD: white, white color-by-atom; sterol: purple color-by-atom; PDB ID 3L0L),¹⁷ viewed along the helix 10/11 axis. The benzyl-pyrazole moiety of compound **28** precludes the agonist conformation of His479.

Larger substituents at the 3-position of the quinoline core can disrupt the His479-Phe502-Tyr506 interaction, leading to full inverse agonism. As with the (*S*)-enantiomers of compounds **12** and **20**, the structure of the LBD-**28** complex was determined, in this case at 3.2Å resolution. In this complex, the pyrazol-1-yl substituent on the benzyl group displaces His479 from its position in the sterol agonist complex structure (Figure 5). It is likely that this obvious steric incompatibility

leads to the complete disruption of helix 10/11 observed in this complex structure, which in turn disturbs helices 11' and 12 and ultimately precludes co-activator and co-repressor binding. Thus, compound **28** and related molecules function as full inverse agonists in our cell-based assay.

To understand the correlation in functional activity between the transfected cell-based reporter assay and relevant human primary cells, we tested a selection of compounds in a Th17 cell assay that measures production of IL-17A under conditions that favor Th17 cell differentiation (Table 5). Compound **20** was found to be an agonist in both the reporter assay and the Th17 cell assay. Compounds **22** and **25**, behaving like neutral antagonists in the reporter assay with less potency than expected when compared to TF binding, also showed less potency in the Th17 cells with inhibition curves only starting to develop at high compound concentrations. Compounds **23** and **27**, containing a 4-trifluoromethylbenzyl substituent, were full inverse agonists in the reporter assay (>100% inhibition at 6 μ M compound concentration), and showed 83% and 95% inhibition in Th17 cells, respectively, a slight reduction in efficacy. This same pattern was observed for compounds **24**, **26** and **28**, which displayed full inverse agonism in the cell-based reporter assay with a reduction in efficacy in the Th17 assay (ranging from 65 to 87% inhibition). All compounds tested showed similar potency in the reporter assay and Th17 assays, except for compound **20** which was 5-fold less potent in Th17 cells compared to the reporter assay. These data support the concept that the cell-based reporter assay is showing a good correlation to the Th17 cell assay, with minor to moderate differences in efficacy in some cases.

Table 5. Functional activity correlation between the transfected cell-based reporter assay and relevant human primary cells.

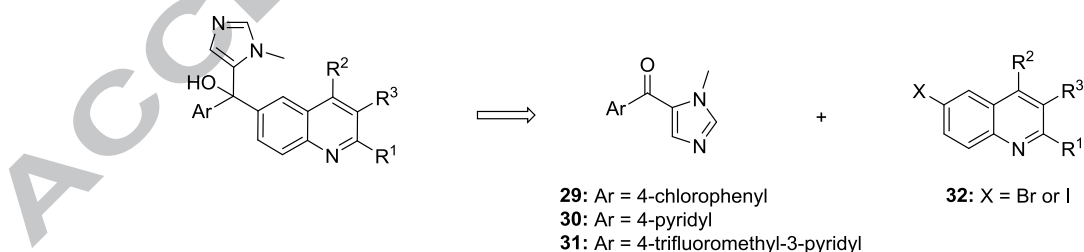
Cmpd ^a	ROR γ t reporter cell assay IC ₅₀ (μ M) (% inh. @ 6 μ M)	Human Th17 assay IC ₅₀ (% inh. ^b @ 6 μ M)
20	0.049 ^c (78)	0.24 (85) ^{c, d}
22	~6 (42)	2.74 (78)
23	0.12 (102)	0.053 (83) ^d
24	0.089 (97)	0.057 (78)
25	~6 (62)	0.42 (78)
26	0.14 (94)	0.045 (65) ^d
27	0.041 (103)	0.062 (95) ^d
28	0.073 (99)	0.085 (87)

^aCmpd = compound; ^binh = inhibition; ^cdenotes EC₅₀ (% increase in transcription activity); ^ddenotes % inhibition at 1.2 μ M instead of 6 μ M.

Structural information has been valuable in furthering our understanding of the SAR in our optimization of this series of quinoline tertiary alcohols. Three crystal structures of the ROR γ t LBD complexed with analogs of this chemotype are generally consistent with the observed functional activities, and provide mechanistic insights into the range of functional activities we describe. The structure of the LBD-**28** complex is, perhaps, the most straightforward of the three to understand. Compound **28** functions as a full inverse agonist by preventing co-activator or co-repressor binding through disruption of the conformation of the helix 10-12 region via a steric clash with the protein in the region of His479. We report an agonist, **20**, that slightly disturbs His479 from the conformation observed in the sterol agonist complex. We speculate that this

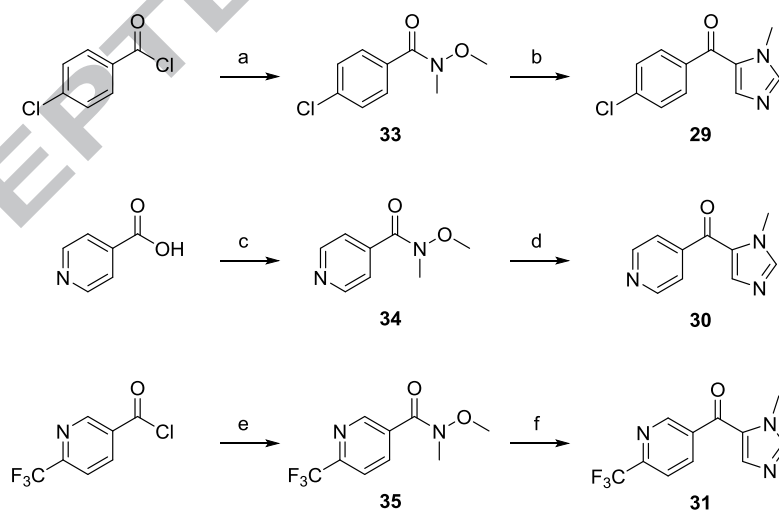
ligand stabilizes a conformation of helix 10/11 that is competent to allow or facilitate binding of co-activator. The complex with the S-enantiomer of compound **12** is especially interesting. Comparison of the LBD-**12** and LBD-sterol complexes indicates that bound compound **12** has no obvious steric clash with the sterol agonist conformation of the LBD that would cause the observed structural changes, yet this compound disrupts agonist conformation and functions as a full inverse agonist in the cell-based reporter assay. Comparison of functional data generated in the cell-based reporter assay versus the Th17 assay shows a trend that suggests the potency is similar between the two assays, however, some subtle differences in efficacy were noted.

Synthetic routes to racemic quinoline tertiary alcohols²⁵⁻²⁸ utilized a key carbon-carbon bond forming reaction between two intermediates; diaryl ketones **29–31** and an organometallic reagent derived from 6-haloquinolines (**32**) (Scheme 1). In this section we detail reaction conditions for the synthesis of these components, their coupling and further elaboration into final product analogs described herein.



Scheme 1. Retrosynthetic route to racemic quinoline tertiary alcohols.

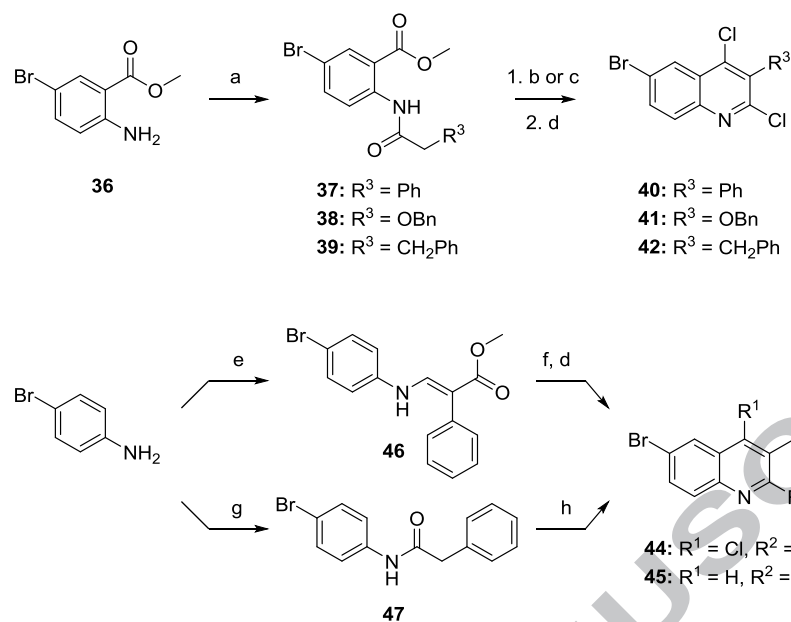
Synthesis of ketone and quinoline intermediates. The synthesis of ketones **29–31** is summarized in Scheme 2. 4-Chlorobenzoyl chloride, 4-picolinic acid, and 6-(trifluoromethyl)nicotinoyl chloride were transformed into the corresponding *N,O*-dimethyl hydroxamic acid derivatives **33–35**, respectively. The reaction conditions and precursor material used to introduce the *N*-methyl imidazole group varied slightly. For example, Grignard reagents derived from 5-bromo-1-methyl-1*H*-imidazole were coupled with amides **33** and **35** to afford ketones **29** and **31**, respectively. The organometallic reagent precursor needed for the synthesis of 4-pyridyl ketone **30** was formed by a deprotonation–protection–deprotonation sequence. First, deprotonation of the C2-position of 1-methyl-1*H*-imidazole with *n*-BuLi and trapping with chlorotriethylsilane followed by a second deprotonation of the C5-position of 1-methyl-2-(triethylsilyl)-1*H*-imidazole with *n*-BuLi provided the requisite C5-lithio imidazole which was coupled with amide **34** to afford ketone **30** (the triethylsilyl protecting group was removed during aqueous workup).



Scheme 2. Synthesis of ketone intermediates. Reagents and reaction conditions: (a) *N,O*-dimethylhydroxylamine hydrochloride, pyridine, CH_2Cl_2 ; (b) 5-bromo-1-methyl-1*H*-imidazole, EtMgBr, THF; (c) *N,O*-dimethylhydroxylamine hydrochloride, CDI, CH_2Cl_2 ; (d) 1-

methyl-1*H*-imidazole, *n*-BuLi, TESCl, $-78\text{ }^{\circ}\text{C}$; then *n*-BuLi, $10\text{ }^{\circ}\text{C}$; then **34**, $-78\text{ }^{\circ}\text{C}$; (e) *N,O*-dimethylhydroxylamine hydrochloride, (*i*-Pr)₂EtN, CH₂Cl₂; (f) 5-bromo-1-methyl-1*H*-imidazole, *i*-PrMgCl•LiCl, THF.

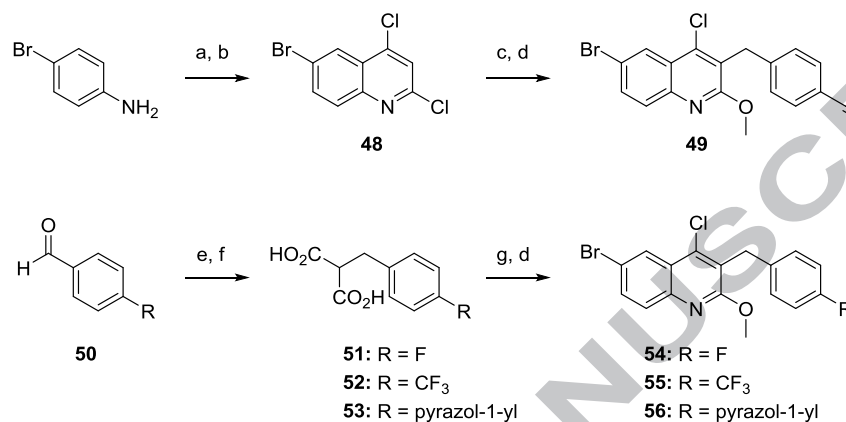
The second precursor required for racemic tertiary alcohol formation was a substituted 6-bromoquinoline compound. Acylation of methyl 2-amino-5-bromobenzoate (**36**) with phenyl acetyl chloride, benzyloxy acetyl chloride or 3-phenylpropanoyl chloride provided amides **37**, **38** and **39**, respectively (Scheme 3). Base-mediated cyclization followed by chlorination with phosphorus oxychloride afforded 6-bromo-2,4-dichloro-quinolines **40–42**. Synthesis of monochloro-substituted quinolines **46** and **47** began by coupling of 4-bromoaniline with ethyl 3-oxo-2-phenylpropanoate or 2-phenylacetyl chloride to afford **44** and **45**, respectively. Cyclization of **46** with polyphosphoric acid and subsequent chlorination provided quinoline **44**. Cyclization of **47** with phosphorus oxychloride in the presence of dimethyl formamide furnished quinoline **45**.



Scheme 3. Synthesis of 6-bromoquinoline intermediates. Reagents and reaction conditions: (a) 2-phenylacetyl chloride, benzyloxyacetyl chloride, or 3-phenylpropanoyl chloride; Et_3N , CH_2Cl_2 ; (b) LiHMDS, THF for amide **37**; (c) KHMDS, THF for amides **38** and **39**; (d) POCl_3 ; (e) ethyl 3-oxo-2-phenylpropanoate, EtOH; (f) PPA, 150°C ; (g) 2-phenylacetyl chloride, Et_3N , DMAP, DCM; (h) POCl_3 , DMF.

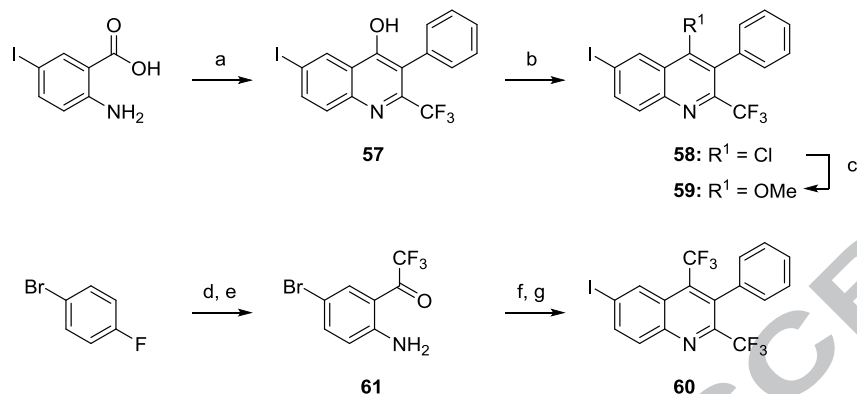
Two additional methods which were utilized to form 6-bromoquinolines are described in Scheme 4. Condensation/cyclization of 4-bromoaniline with 2,2-dimethyl-1,3-dioxan-4,6-dione followed by chlorination with phosphorus oxychloride afforded dichloroquinoline **48**. Deprotonation of the C3-position of **48** with LDA and coupling with 4-(bromomethyl)benzotrile provided **49** after methoxylation of the C2-position of the core. Alternatively, the 1,3-dicarboxylic acids **51-53** could be synthesized by a condensation/reduction sequence between 4-substituted benzaldehydes **50** and 2,2-dimethyl-1,3-dioxan-4,6-dione using catalytic proline and the stoichiometric reducing reagent diethyl 1,4-dihydro-2,6-dimethyl-3,5-pyridinedicarboxylate²⁹

followed by base- or acid-mediated hydrolysis. Condensation/cyclization with 4-bromoaniline, chlorination, and methoxylation afforded quinolines **54–56**.



Scheme 4. Synthesis of 6-bromoquinoline intermediates. Reagents and reaction conditions: (a) 2,2-dimethyl-1,3-dioxan-4,6-dione; then Eaton's reagent; (b) POCl₃; (c) LDA, 4-(bromomethyl)benzotrile, THF; (d) NaOMe; (e) 2,2-dimethyl-1,3-dioxane-4,6-dione, catalytic L-proline, EtOH; then diethyl 1,4-dihydro-2,6-dimethyl-3,5-pyridinedicarboxylate; (f) aqueous NaOH for **51** and **53**; aqueous TFA for **52**; (g) 4-bromoaniline, POCl₃.

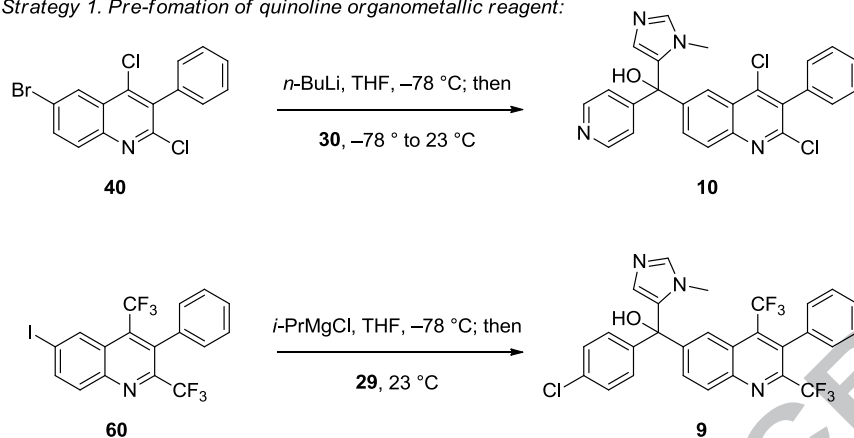
The synthesis of trifluoromethyl-substituted quinolines is described in Scheme 5. Cyclization of 2-amino-5-iodo-benzoic acid with 1,1,1-trifluoro-3-phenylpropan-2-one and Eaton's reagent afforded hydroxyl quinoline **57**. Chlorination with phosphorus oxychloride followed by methoxylation furnished iodoquinoline **59**. Synthesis of 2,4-bistrifluoromethyl quinoline **60** proceeded by a four step sequence starting with deprotonation of 1-bromo-4-fluorobenzene with LDA and coupling of the formed aryl lithium reagent with ethyl trifluoroacetate. A two-step, one-pot azidation–reduction reaction provided aniline **61**. Cyclization with 1,1,1-trifluoro-3-phenylpropan-2-one in hot DMF in the presence of tributylamine and a subsequent iodination completed the synthesis of quinoline **60**.



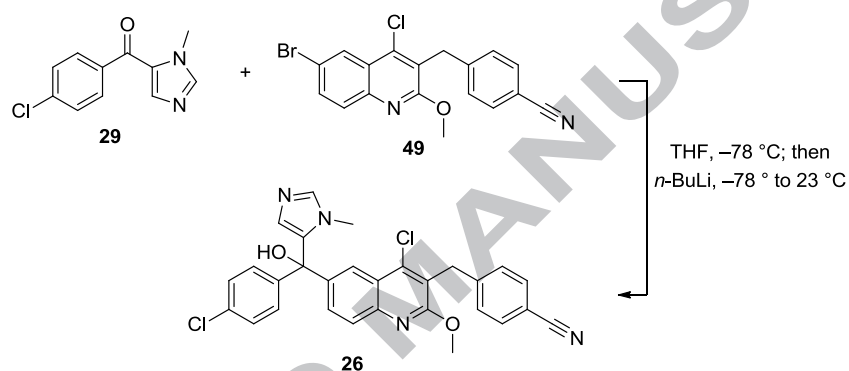
Scheme 5. Synthesis of trifluoromethyl-substituted quinoline intermediates. Reagents and reaction conditions: (a) 1,1,1-trifluoro-3-phenylpropan-2-one, Eaton's reagent, 100 °C; (b) POCl₃, 110 °C; (c) NaOCH₃/CH₃OH; (d) LDA, THF, -78 °C; then ethyl trifluoroacetate, 23 °C; (e) NaN₃, DMSO, 95 °C; then SnCl₂•dihydrate; (f) 1,1,1-trifluoro-3-phenylpropan-2-one, DMF, Bu₃N, 130 °C; (g) CuI, DMEDA, t-BuOH, NaI, microwave, 150 °C.

Tertiary alcohol formation reaction conditions. Tertiary alcohol construction relied on a carbon-carbon bond forming reaction between a diaryl ketone and an organometallic reagent derived from a 6-halo quinoline. This synthetic step was executed using two strategies as exemplified in Scheme 6. In the first, the diaryl ketone component was added to a pre-formed organometallic reagent derived from 6-bromo or -iodo quinolines **40** and **60** using *n*-butyllithium or *i*-propylmagnesium chloride, respectively, at low temperature (-78 °C). In the second method, *n*-butyllithium was added to a -78 °C solution of ketone **29** and quinoline **49** in tetrahydrofuran (*in-situ coupling conditions*). These methods were applied to the synthesis of other quinoline tertiary alcohols described herein.

Strategy 1. Pre-formation of quinoline organometallic reagent:



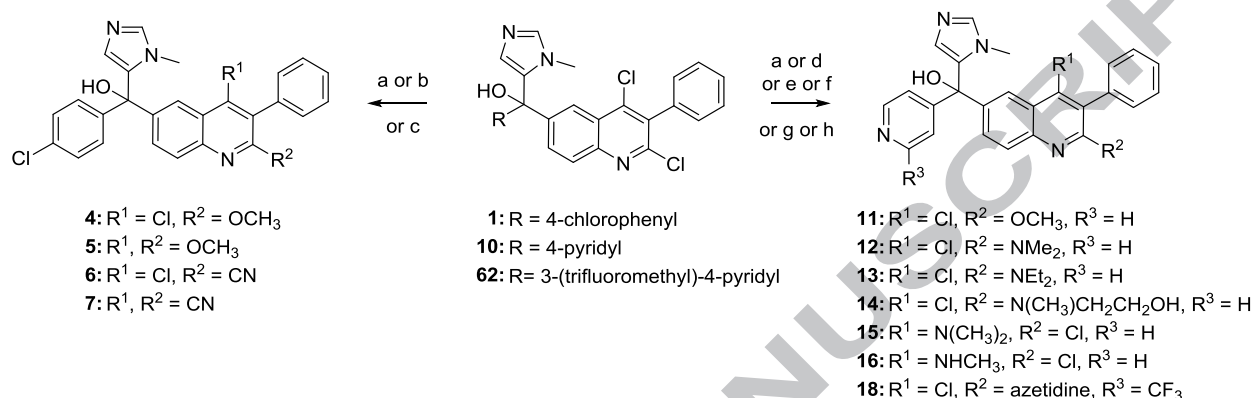
Strategy 2. In-situ coupling:



Scheme 6. Tertiary alcohol synthesis.

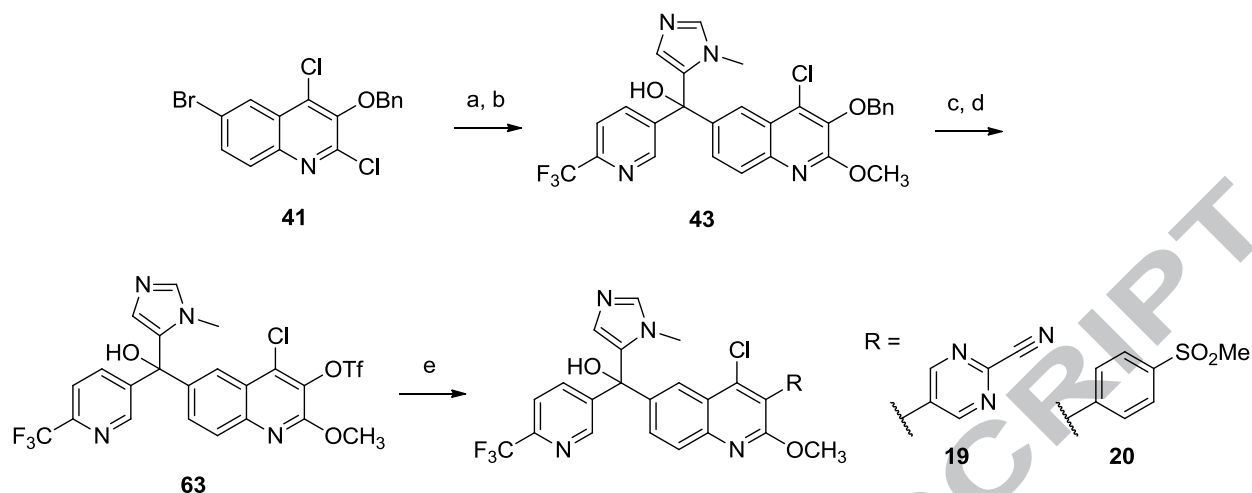
Transformations of quinoline tertiary alcohols. The chlorine atoms of 2,4-dichloroquinolines **1**, **10**, and **62** can be replaced with numerous groups as described in Scheme 7. Selective displacement of the C2-chlorine atom with methoxide proceeds in hot toluene^{30,31} (compounds **4** and **11**) whereas replacement of both chlorine atoms requires methoxide in hot methanol (compound **5**). The introduction of nitrile groups was also achieved in a selective manner; the substitution of the C2-chlorine atom proceeded within 4 hours and the substitution of both chlorine atoms in 22 hours under palladium-catalyzed cyanation reaction conditions (compounds **6** and **7**). Reaction conditions that installed amino groups gave rise to C2-amino quinoline

products as the major products (compounds **12**, **13**, **14** and **18**) and in two instances the C4-amino product was isolated (compounds **15** and **16**).



Scheme 7. Displacement of chlorine atoms. Reagents and reaction conditions: (a) NaOCH_3 (excess), toluene, reflux; (b) NaOMe (excess), methanol, reflux; (c) Pd_2dba_3 , dppf , $\text{Zn}(\text{CN})_2$, zinc nanopowder, DMA, 120°C , 4 hr (22 hr to displace both chlorine atoms); (d) $2\text{M NH}(\text{CH}_3)_2$ in MeOH, 80°C ; (e) NHEt_2 , DMF, 130°C ; (f) 2-(methylamino)ethanol, 80°C , 16 hr; (g) 33% CH_3NH_2 in EtOH, TFA, 80°C , 17 hr; (h) azetidone, DMF, 100°C ; then chiral SFC separation.

The synthesis of quinoline tertiary alcohols **19** and **20** was accomplished by way of palladium-catalyzed cross coupling reactions between triflate **63** and (4-(methylsulfonyl)phenyl)boronic acid or 5-(4,4,5,5-tetramethyl-1,3,2-dioxaborolan-2-yl)pyrimidine-2-carbonitrile (Scheme 8).



Scheme 8. Synthesis of quinoline tertiary alcohols **19** and **20**. Reagents and reaction conditions: (a) *n*-BuLi, THF, $-78\text{ }^{\circ}\text{C}$; then **31**, -78 ° to $0\text{ }^{\circ}\text{C}$; (b) NaOMe, MeOH; (c) H_2 , 10% Pd/C, CH_3OH , 1.5 hr; (d) trifluoromethanesulfonic anhydride, pyridine; (e) (4-(methylsulfonyl)phenyl)boronic acid or 5-(4,4,5,5-tetramethyl-1,3,2-dioxaborolan-2-yl)pyrimidine-2-carbonitrile, $\text{PdCl}_2(\text{dppf})$, K_2CO_3 , 1,4-dioxane, $65\text{ }^{\circ}\text{C}$, 15 hr.

1. Jetten, A. M. *Nucl Recept Signal* **2009**, 7, e003.
2. Ivanov, I. I.; McKenzie, B. S.; Zhou, L.; Tadokoro, C. E.; Lepelley, A.; Lafaille, J. J.; Cua, D. J.; Littman, D. R. *Cell* **2006**, 126, 1121-1133.
3. Elloso, M. M.; Gomez-Angelats, M.; Fourie, A. M. *J Leukoc Biol* **2012**, 92, 1187-1197.
4. Rizvi, S.; Chaudhari, K.; Syed, B. A. *Nat Rev Drug Discov* **2015**, 14, 745-746.
5. Chabaud, M.; Durand, J. M.; Buchs, N.; Fossiez, F.; Page, G.; Frappart, L.; Miossec, P. *Arthritis Rheum* **1999**, 42, 963-970.
6. Kotake, S.; Udagawa, N.; Takahashi, N.; Matsuzaki, K.; Itoh, K.; Ishiyama, S.; Saito, S.; Inoue, K.; Kamatani, N.; Gillespie, M. T.; Martin, T. J.; Suda, T. *J Clin Invest* **1999**, 103, 1345-1352.
7. Sarra, M.; Pallone, F.; Macdonald, T. T.; Monteleone, G. *Inflamm Bowel Dis* **2010**, 16, 1808-1813.
8. Komiyama, Y.; Nakae, S.; Matsuki, T.; Nambu, A.; Ishigame, H.; Kakuta, S.; Sudo, K.; Iwakura, Y. *J Immunol* **2006**, 177, 566-573.
9. Cyr, P.; Bronner, S. M.; Crawford, J. J. *Bioorg Med Chem Lett* **2016**, 26, 4387-4393.
10. Fauber, B. P.; Magnuson, S. *J Med Chem* **2014**, 57, 5871-5892.
11. Kojetin, D. J.; Burris, T. P. *Nat Rev Drug Discov* **2014**, 13, 197-216.
12. Zhang, Y.; Luo, X. Y.; Wu, D. H.; Xu, Y. *Acta Pharmacol Sin* **2015**, 36, 71-87.
13. Germain, P.; Staels, B.; Dacquet, C.; Spedding, M.; Laudet, V. *Pharmacol Rev* **2006**, 58, 685-704.
14. Wang, Y.; Kumar, N.; Nuhant, P.; Cameron, M. D.; Istrate, M. A.; Roush, W. R.; Griffin, P. R.; Burris, T. P. *ACS Chem Biol* **2010**, 5, 1029-1034.

15. Solt, L. A.; Kumar, N.; Nuhant, P.; Wang, Y.; Lauer, J. L.; Liu, J.; Istrate, M. A.; Kamenecka, T. M.; Roush, W. R.; Vidovic, D.; Schurer, S. C.; Xu, J.; Wagoner, G.; Drew, P. D.; Griffin, P. R.; Burriss, T. P. *Nature* **2011**, *472*, 491-494.
16. ROR γ and ROR γ t differ only at the N-terminus; the DNA and ligand binding domains of ROR γ and ROR γ t are identical.^{1,32} Throughout this paper we will use the term ROR γ t ligand binding domain (LBD) to refer to the LBD of both ROR γ and ROR γ t.
17. Jin, L.; Martynowski, D.; Zheng, S.; Wada, T.; Xie, W.; Li, Y. *Mol Endocrinol* **2010**, *24*, 923-929.
18. Huh, J. R.; Leung, M. W.; Huang, P.; Ryan, D. A.; Krout, M. R.; Malapaka, R. R.; Chow, J.; Manel, N.; Ciofani, M.; Kim, S. V.; Cuesta, A.; Santori, F. R.; Lafaille, J. J.; Xu, H. E.; Gin, D. Y.; Rastinejad, F.; Littman, D. R. *Nature* **2011**, *472*, 486-490.
19. Rene, O.; Fauber, B. P.; Boenig Gde, L.; Burton, B.; Eidenschenk, C.; Everett, C.; Gobbi, A.; Hymowitz, S. G.; Johnson, A. R.; Kiefer, J. R.; Liimatta, M.; Lockey, P.; Norman, M.; Ouyang, W.; Wallweber, H. A.; Wong, H. *ACS Med Chem Lett* **2015**, *6*, 276-281.
20. Fujita-Sato, S.; Ito, S.; Isobe, T.; Ohyama, T.; Wakabayashi, K.; Morishita, K.; Ando, O.; Isono, F. *Journal of Biological Chemistry* **2011**, *286*, 31409-31417.
21. Matulis, D.; Kranz, J. K.; Salemme, F. R.; Todd, M. J. *Biochemistry* **2005**, *44*, 5258-5266.
22. Soroosh, P.; Wu, J.; Xue, X.; Song, J.; Sutton, S. W.; Sablad, M.; Yu, J.; Nelen, M. I.; Liu, X.; Castro, G.; Luna, R.; Crawford, S.; Banie, H.; Dandridge, R. A.; Deng, X.; Bittner, A.; Kuei, C.; Tootoonchi, M.; Rozenkrants, N.; Herman, K.; Gao, J.; Yang, X. V.; Sachen, K.; Ngo, K.; Fung-Leung, W. P.; Nguyen, S.; de Leon-Tabaldo, A.; Blevitt, J.; Zhang, Y.; Cummings, M. D.; Rao, T.; Mani, N. S.; Liu, C.; McKinnon, M.; Milla, M. E.; Fourie, A. M.; Sun, S. *Proc Natl Acad Sci U S A* **2014**, *111*, 12163-12168.
23. Olsson, R. I.; Xue, Y.; von Berg, S.; Aagaard, A.; McPheat, J.; Hansson, E. L.; Bernstrom, J.; Hansson, P.; Jirholt, J.; Grindebacke, H.; Leffler, A.; Chen, R.; Xiong, Y.; Ge, H.; Hansson, T. G.; Narjes, F. *ChemMedChem* **2016**, *11*, 207-216.
24. Huang, P.; Chandra, V.; Rastinejad, F. *Annu Rev Physiol* **2010**, *72*, 247-272.
25. Leonard, K. A.; Barbay, K.; Edwards, J. P.; Kreutter, K. D.; Kummer, D. A.; Maharoo, U.; Nishimura, R.; Urbanski, M.; Venkatesan, H.; Wang, A.; Wolin, R. L.; Woods, C. R.; Cummings, M. D.; Janssen Pharmaceutica NV, Belgium; 2016; US patent 9,403,816 B2.
26. Leonard, K. A.; Barbay, K.; Edwards, J. P.; Kreutter, K. D.; Kummer, D. A.; Maharoo, U.; Nishimura, R.; Urbanski, M.; Venkatesan, H.; Wang, A.; Wolin, R. L.; Woods, C. R.; Fourie, A.; Xue, X.; Cummings, M. D.; Jones, W. M.; Goldberg, S.; Janssen Pharmaceutica NV, Belgium; 2016; US Patent 9,284,308 B2.
27. Leonard, K. A.; Barbay, K.; Edwards, J. P.; Kreutter, K. D.; Kummer, D. A.; Maharoo, U.; Nishimura, R.; Urbanski, M.; Venkatesan, H.; Wang, A.; Wolin, R. L.; Woods, C. R.; Fourie, A.; Xue, X.; Mirzadegan, T.; Ganamet, K.; Janssen Pharmaceutica NV, Belgium; 2016; US Patent 9,309,222 B2.
28. Leonard, K. A.; Barbay, K.; Edwards, J. P.; Kreutter, K. D.; Kummer, D. A.; Maharoo, U.; Nishimura, R.; Urbanski, M.; Venkatesan, H.; Wang, A.; Wolin, R. L.; Woods, C. R.; Pierce, J.; Goldberg, S.; Fourie, A.; Xue, X.; Janssen Pharmaceutica NV, Belgium; 2016; US Patent 9,290,476 B2.

29. Ramachary, D. B.; Kishor, M.; Ramakumar, K. *Tetrahedron Letters* **2006**, *47*, 651-656.
30. Osborne, A. G.; Dimitrova, G. T.; Galbally, P.; Hughes, D. D.; Jones, C.; Lipman, A. L.; Wilstead, N. *J. Chem. Res., Synop.* **2002**, *4*, 0124-0148.
31. Osborne, A. G.; Miller, L. A. D. *J. Chem. Soc., Perkin Trans. 1* **1993**, 181-184.
32. Villey, I.; de Chasseval, R.; de Villartay, J. P. *Eur J Immunol* **1999**, *29*, 4072-4080.

Graphical abstract:

